Surface Mesoscale Processes during the 1994 Palm Sunday Tornado Outbreak

ADAM H. LANGMAID AND ALLEN J. RIORDAN

Department of Marine, Earth, and Atmospheric Sciences, North Carolina State University, Raleigh, North Carolina

(Manuscript received 6 January 1997, in final form 31 December 1997)

ABSTRACT

The tornadic storms that developed in the 27 March 1994 Palm Sunday outbreak were confined to a narrow zone extending from central and northern Alabama to western North Carolina. Analysis of surface observations and soundings is used to examine the mesoscale environment of the region starting 14 h prior to storm development. The evolution of a shallow front that formed the northern boundary of the outbreak region is tied to several diabatic processes including evaporation of precipitation and differential solar heating. The resulting front was found to both limit severe convection and focus supercell development later in the day.

During the night before the outbreak, as copious widespread precipitation fell into dry air, evaporation maintained a cold air pool north of the front. By contrast, moderate southerly flow provided warm, moist conditions to the south. Precipitation-enhanced cold air damming along the eastern slopes of the Appalachians also may have provided a source of cold air for subsequent frontogenesis over areas farther west. During the daylight hours, differential solar heating across the front further enhanced frontogenesis.

Intensification of convection just prior to the first tornadoes was found to be associated with areas of breaks in the overcast near and upstream of tornadogenesis. Similarly, cells that intensified were moving over a surface that had been thoroughly moistened by previous rainfall. Supercells that intersected and moved along the frontal boundary maintained their tornadic strength for many hours, whereas storms that crossed the boundary disintegrated. Blockage of inflow by upstream storm cells may also have contributed to the rapid reduction of intensity of one of the tornadic cells.

1. Introduction

On 27 March 1994 (Palm Sunday), an outbreak of severe storms (producing about 30 tornadoes, devastating winds, and large hail) swept through Alabama, Georgia, and the Carolinas, resulting in 42 deaths, over 300 injuries, and damage of over $100 million. The severe weather was concentrated mostly in a narrow path roughly 50 km wide and over 570 km long, extending from central Alabama to south-central North Carolina. The paths of several of the tornadoes in Georgia originated from separate convective systems. However, many of these tornadoes followed similar tracks (Fig. 1).

Studies in this issue by Koch et al. (1998) and Hamilton et al. (1998) show that the Palm Sunday environment did not exhibit the classical structure often associated with severe weather outbreaks (Miller 1972). Rather, the event may have been triggered by an unbalanced mesoscale jetlet that moved into the region from the southwest and organized the development of convective lines in an environment characterized by asymmetric inertial instability.

It is the purpose of this study to focus on mesoscale processes at and near the surface and to document the detailed structure and evolution of observed thermal and moisture boundaries. Such features may have triggered the tornadic storm development or confined the outbreak to its observed narrow swath. Part of the purpose of this paper is to investigate the role of diabatic heating in producing or maintaining the mesoscale structures that led to the severe outbreak.

Surface mesoscale boundaries vary considerably in their origin and evolution. For example, some form when cool stable air is trapped by local topography (Businger et al. 1991; Keeter et al. 1995) or by precipitation-induced evaporational cooling (Fritsch et al. 1992). Rain-cooled boundaries similar to convective outflows can increase the thermal gradient and form shallow fronts. Korotky (1990), Businger et al. (1991), and Vescio et al. (1993) have emphasized the importance of such shallow features in focusing severe convection in the Southeast.

Numerous observational and simulation studies have demonstrated that diabatic influences may significantly intensify frontogenesis (Koch 1984; Dorian and Koch 1988; Businger et al. 1991). Gyakum and Barker (1988) used standard AFOS hourly observations to show how

Corresponding author address: Dr. Al Riordan, Dept. of Marine, Earth, and Atmospheric Sciences, Box 8208, North Carolina State University, Raleigh, NC 27695-8208.
E-mail: al_riordan@ncsu.edu

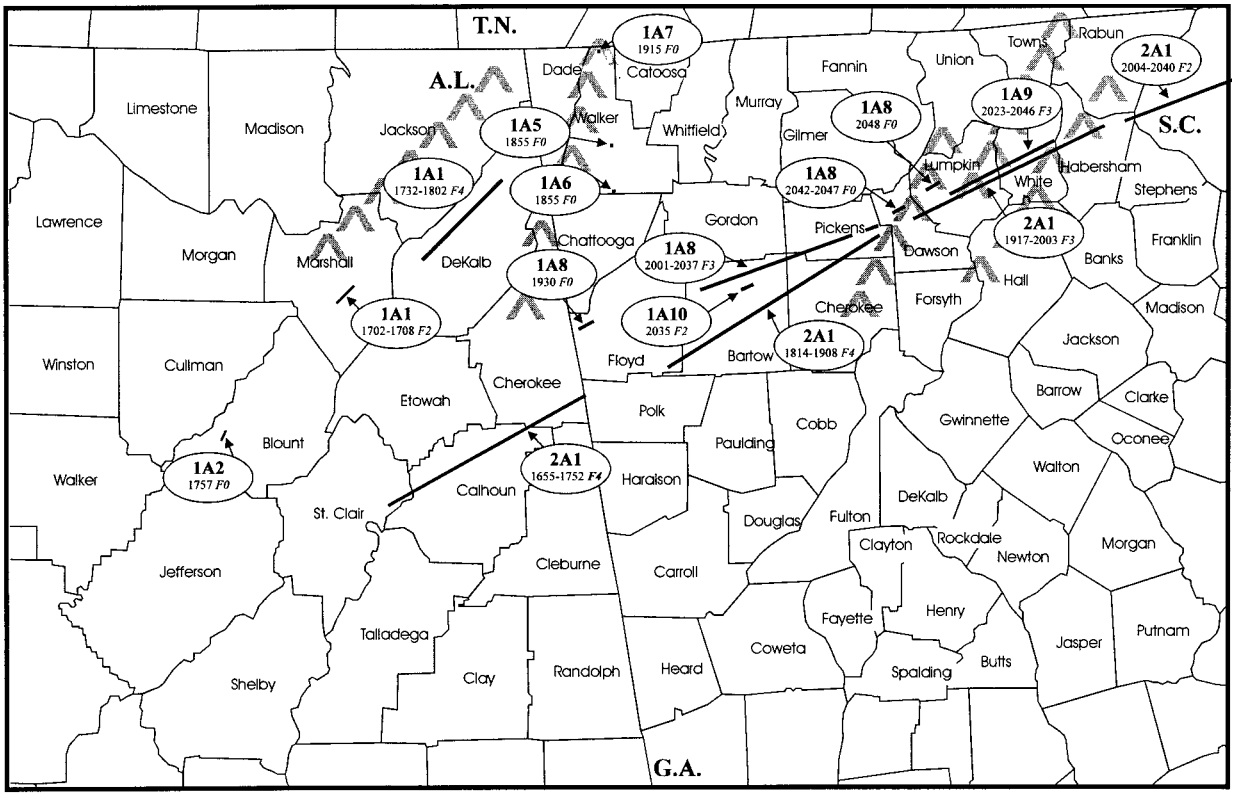

FIG. 1. Tornado tracks (solid lines) from MCS 1A and 2A in Alabama and Georgia. Parent cell (bold), time (UTC), and F number are encircled. The southern extensions of the Appalachian Mountains are represented by inverted ''V'' symbols.

mesoscale solar heating differences across a surface cold front enhance surface frontogenesis and may aid mesoscale cyclogenesis. Nonclassical, thermally forced mesoscale circulations may arise from horizontal gradients in sensible heat flux in the planetary boundary layer (PBL). Zhang and Anthes (1982) suggested that soil moisture is most influential in modifying sensible heat fluxes. Two-dimensional numerical modeling studies by Segal et al. (1986), Segal et al. (1989), Segal et al. (1992), and Segal et al. (1993) show how differential cloud cover or soil moisture contrasts may result in a solenoidal circulation comparable to a sea breeze. Sun and Ogura (1979) determined that differential heating may be capable of forcing vertical motions sufficient to release ambient potential instability responsible for a squall line along a dryline. Segal et al. (1993) found that prolonged cloud shading behind a synoptic cold front can increase surface frontogenesis and can be ignored only for very moist homogeneous summer conditions or snow-covered ground. Thompson and Burk (1991) describe how sensible heating, when occurring in the cold air behind the Arctic front, weakens frontogenesis. Koch et al. (1995) demonstrated that, for a variety of model configurations, frontogenesis is dominated by surface confluence and although the direct contribution by the diabatic term is secondary, a nonlinear relationship exists between the adiabatic frontal circulation and the circulation forced by diabatic effects. The relationship between surface deformation and diabatic frontogenesis has been suggested as a possible trigger for frontal squall lines (Koch 1984; Dorian and Koch 1988). Koch et al. (1997) use a mesoscale model to examine the role of cloud cover in frontogenesis and squall line forcing.

2. Data

This case study employed surface and upper-air observations and satellite and radar imagery. The locations of available surface and upper-air sites are illustrated in Fig. 2. The surface observational network consisted of synoptic hourly reports of temperature, moisture, pressure, and winds from routine sources, plus data from two mesoscale networks: the Alabama mesonet, which augmented synoptic resolution with seven surface sites; and a micro-gamma surface network at Redstone Arsenal (hereafter referred to as RSA), ~8 km south of Huntsville, Alabama. Although RSA sites were too close to Huntsville to truly represent a separate site for mesoscale hand analyses, their data were useful in evaluating the representativeness of the Huntsville reports. In addition, RSA provided 15-min averages of solar radiation. Surface rain gauges, *GOES-7* satellite imagery, and WSI composite radar imagery facilitated iden-

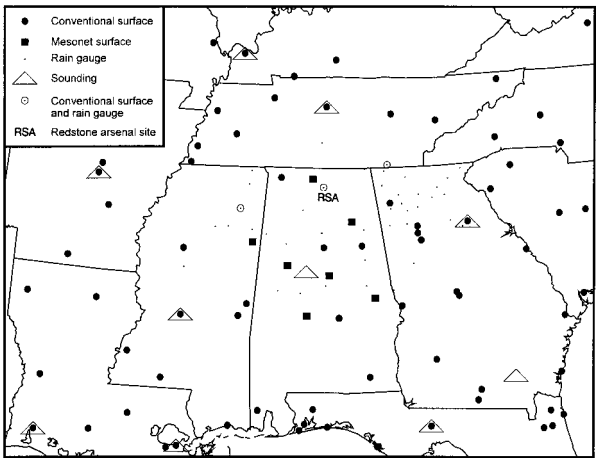

FIG. 2. All available surface and upper-air observations during the period from 0000 UTC 27 March to 0000 UTC 28 March.

tifying boundaries undetectable by conventional observations. Objective analyses used the Barnes objective scheme (Barnes 1973). An ensemble average of the RSA dataset provided a single additional station for these objective analyses and the Alabama mesonet doubled the number of stations in Alabama.

3. Methodology

Hand analyses of surface fronts followed the suggestions given by Sanders and Doswell (1995). Time series of temperature, dewpoint, and winds at individual stations were used to determine the time of frontal passage to within 30 min. Temporal and spatial continuity were then used to obtain the best approximation of the position of the cold front and mesolows. This procedure was especially helpful since several frontal systems and outflow boundaries crossing the same region presented a potentially confusing picture.

Hourly rain gauge totals and radar-derived instantaneous rainfall rates described the influence of prefrontal rainbands in wetting the convective environment. Summing the rain gauge amounts from 0500 to 1200 UTC 27 March, to include the period when widespread rains began in the outbreak region, provided an estimate of available surface moisture.

4. Results

a. Establishing the northern boundary of the outbreak region

Roughly 14 h before deep convection began, a cold front was approaching from the northwest while a weaker, east–west frontal boundary had developed and was slowly moving north (Fig. 3). As will be demonstrated, this latter important feature was maintained chiefly by a combination of processes including differential cooling by evaporation of precipitation and differential solar heating.

At 0000 UTC, the weak east–west front can be seen across Alabama and Georgia. Farther east, over South Carolina, the thermal gradient was weaker, but surface wind and pressure reports suggest that a trough extended northeast into North Carolina. The inverted surface pressure ridge just west of the trough over the western Carolinas appears to be caused by damming of southeasterly flow by the Appalachians. Upper-air analysis (not shown) confirms that the cool air between the two parallel fronts was shallow since no thermal gradient existed in this region at 925 mb.

With a relatively strong pressure gradient and well-established southerly winds across Mississippi and Alabama, one might expect the shallow front west of the mountains to have moved rapidly north allowing warm, moist unstable conditions, and hence the threat of severe weather, to become established as far north as Kentucky. However, the air between the shallow front and the stronger warm front to its north was remarkably dry, with temperature–dewpoint differences of over 10°C over most of the region.

1) WIDESPREAD EVAPORATIVE COOLING

By 0600 UTC and continuing through 0900 UTC (Figs. 4 and 5), a widespread persistent area of precipitation became established over the region between the fronts. Over the next 6–9 h, torrential rain caused major flooding over northern Alabama and flash floods over the eastern third of Tennessee where some areas reported over 17 cm of rainfall. The areal coverage of the precipitation is included in the 0900 UTC analysis. In northern Mississippi and Alabama, the southern margin of the precipitation zone formed three parallel lines (Fig. 5). As these lines swept east across northern Alabama, they established an east–west boundary of differential surface moisture, which was later collocated with severe storm intensification.

A related development between 0000 and 0900 UTC was of more immediate importance in anchoring and intensifying the southern front. First, there is strong evidence that evaporation from precipitation cooled the air north of the front. Figure 6 illustrates time series of hourly reports from Chattanooga, Tennessee (CHA), and Greenville–Spartanburg, South Carolina (GSP), located just north of the front. The onset of rain was associated with increasing dewpoint and decreasing temperature.

If cooling is primarily due to evaporation it can be seen in the evolution of the saturation point at representative stations. Following the method described by Betts (1982, 1984), one computes the saturation point; that is, the temperature and pressure at the lifting condensation level for a surface air parcel. If evaporation is the main cause of cooling, then successive hourly values of the saturation point will descend along a saturated adiabat. The results are plotted in Fig. 7 for Nash-

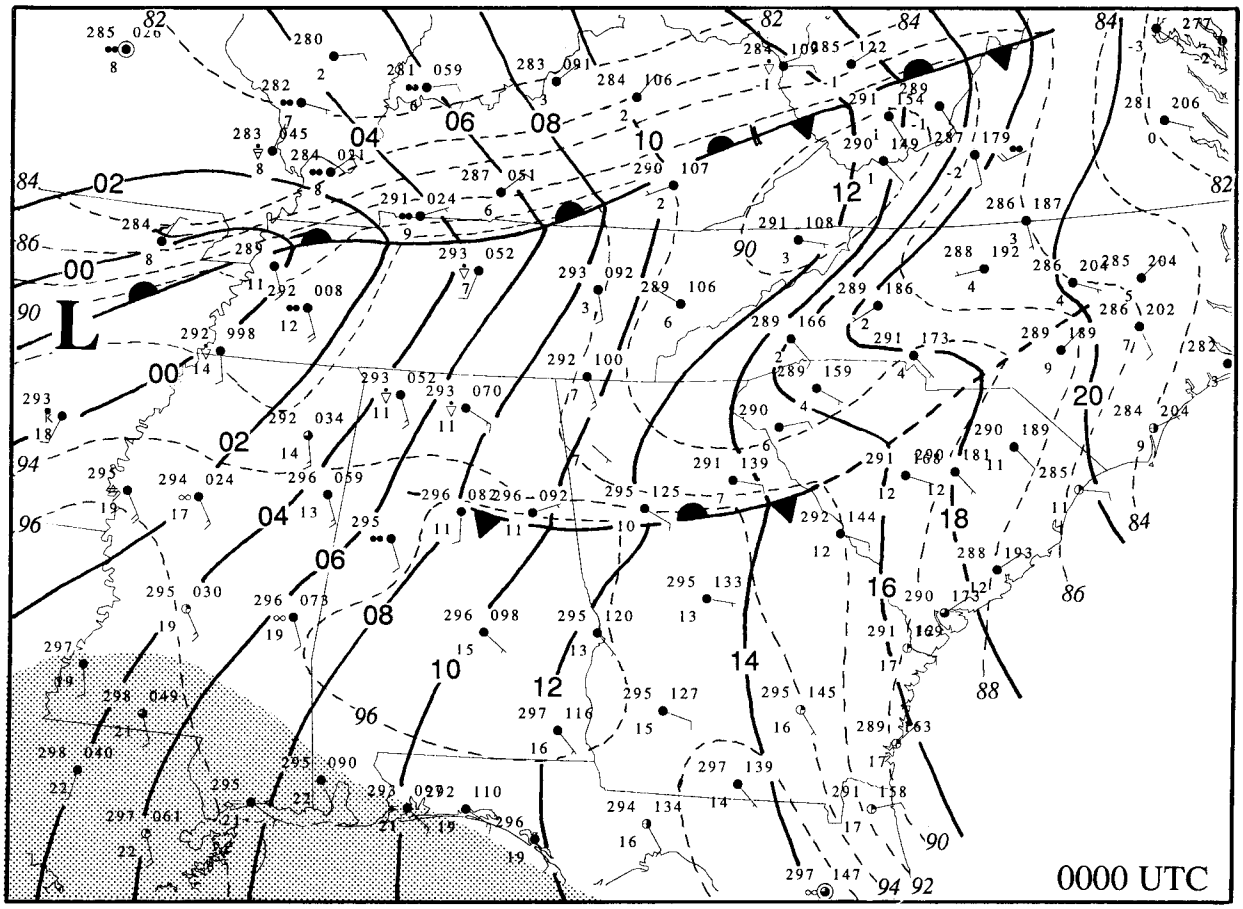

FIG. 3. Surface analysis of sea level pressure (solid lines labeled in mb, minus 1000 mb) and potential temperature (dashed lines labeled in K, minus 200 K) for 27 March 1994 at 0000 UTC. Shading indicates regions with surface dewpoint greater than 20°C. Station data are plotted in the usual fashion except that potential temperature (K) is noted in place of the temperature.

ville, Tennessee, and Hickory, North Carolina, starting at 0000 UTC. Within the margin of error (assuming that observed surface temperatures and dewpoints are representative only to within 1°C), one can reasonably say that evaporation was the most likely cause of cooling for 7 h at Nashville and 4–5 h at Hickory. For the last few hours at each site, especially at Hickory, points are displaced to the right of the moist adiabat. Such a displacement is generally indicative of radiative warming (Betts 1982), in this case, probably due to infrared radiation emitted by the warmer air above the frontal inversion.

2) ADVECTIVE AND DAMMING EFFECTS

While evaporative cooling was shown to be important in maintaining the cold pool north of the front, advective contributions to frontogenesis are often assumed to dominate on the synoptic scale. Such contributions rely on differential advection across the front. Frontogenesis is maximized by cold advection in the cold air and warm advection in the warm air. It is readily apparent from the thermal gradient in Figs. 3–5 that only cold advection north of the front would have been an effective contributor. However, when one also incorporates wind reports and the analyzed pressure field, one finds no systematic cold advection. Objective analysis of the advection rate at two representative stations—CHA and GSP (in Fig. 5)—confirms this impression. Here, between 0200 and 0600 UTC, local cooling rates of up to 3°C h^{-1} contrast dramatically with advective cooling rates one to two orders of magnitude smaller. Advective cooling rates produced by objective analysis typically underestimate the observed local time rate of temperature change, but should be of the correct order of magnitude if large-scale advection is contributing substantially to the observed changes. Thus, the large-scale advective cooling rate is incapable of explaining the observed cooling. Hence, the advective contribution to frontogenesis is negligible.

The damming pool over western North Carolina was weaker and located farther west than in more typical major cases of East Coast damming, as described for example by Bell and Bosart (1988). In our case, the

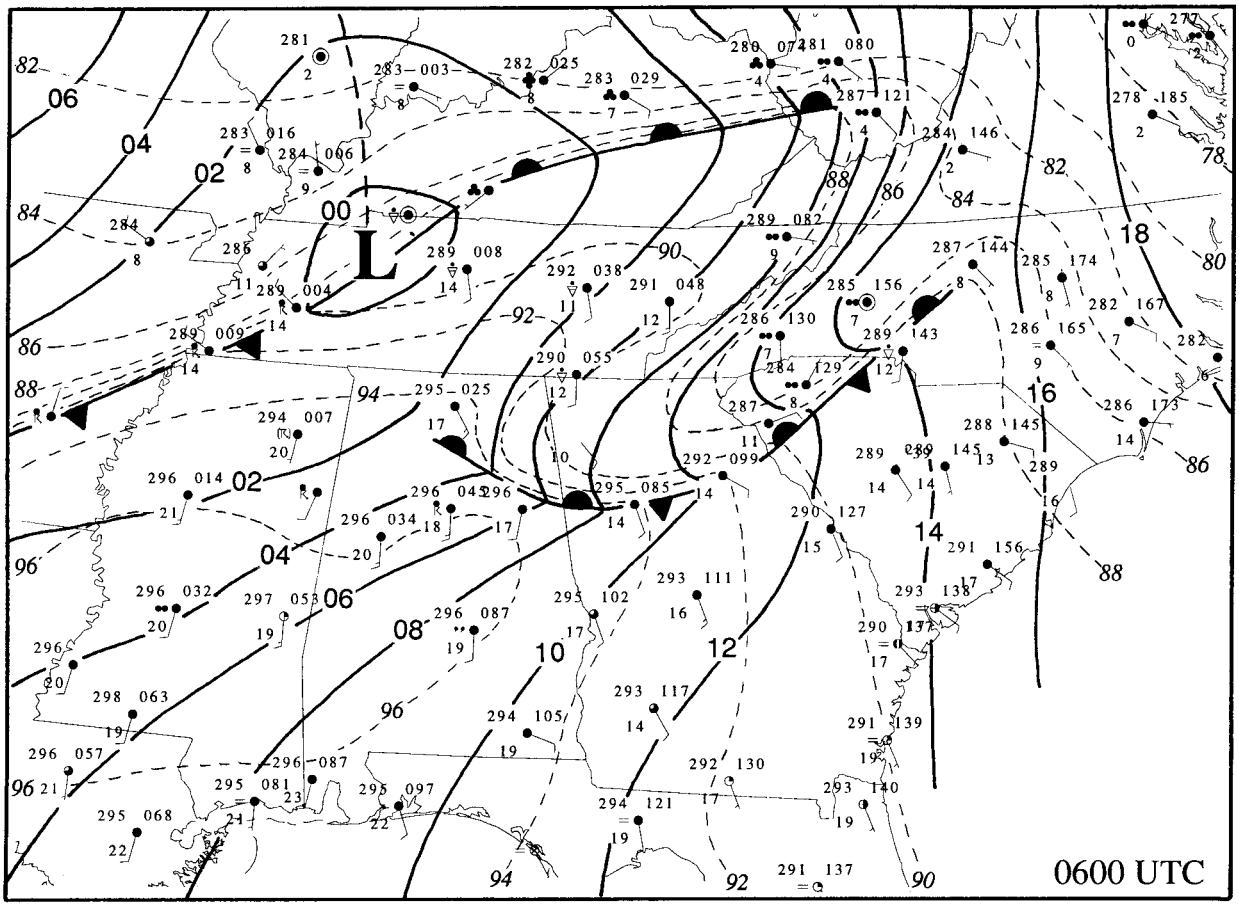

FIG. 4. Same as Fig. 3 but for 0600 UTC and without dewpoint analysis.

prevailing synoptic-scale pressure gradient east of the cold pool was directed almost westward instead of southward. The resulting surface approach flow over the coastal sections of the Carolinas was therefore more southerly, as is typical of dissipating stages of damming. However, precipitation just east of the Appalachians was evidently maintaining the cold pool through evaporative cooling, similar to that described by Fritch et al. (1992) and Bell and Bosart (1988).

Intensification of the inverted ridge associated with the damming may have enhanced a cool flow of air around the southern flank of the Appalachians and into northern Georgia. Similar topographic effects have been documented in this region when cold air streams southwestward into Georgia following major cold front passage from the northwest (O'Handley and Bosart 1996). However, surface wind reports after 0600 UTC do not offer strong support for such flanking flow.

3) FURTHER EVAPORATION AND SOLAR HEATING

Farther west in northern Alabama, the potential temperature gradient weakened after 0000 UTC, and thus, for a time, the front remained weak and ill defined. However, the development of a cool outflow region associated with thunderstorms over northeast Mississippi at 0900 UTC helped reinforce the gradient along the front's western extent. Nevertheless, by 1200 UTC (Fig. 8) the front had weakened considerably across northern Georgia and South Carolina as the damming pool was starting to erode.

By 1500 UTC (Fig. 9), strengthening of the middle section of the front gave it better east–west continuity and established it as a less ephemeral feature. The reason for the frontogenesis is readily apparent by the evolution of the thermal field in the hours after sunrise (cf. Figs. 8 and 9). After 1200 UTC, nearly all areas south of the front warmed, while to the north, temperatures remained generally unchanged. Differential solar heating was likely a chief cause since overcast conditions prevailed north of the front, while broken clouds were found to the south.

b. Static stability

Whereas the east–west frontal boundary was becoming established to form the northern perimeter of the severe weather, water vapor was also dramatically in-

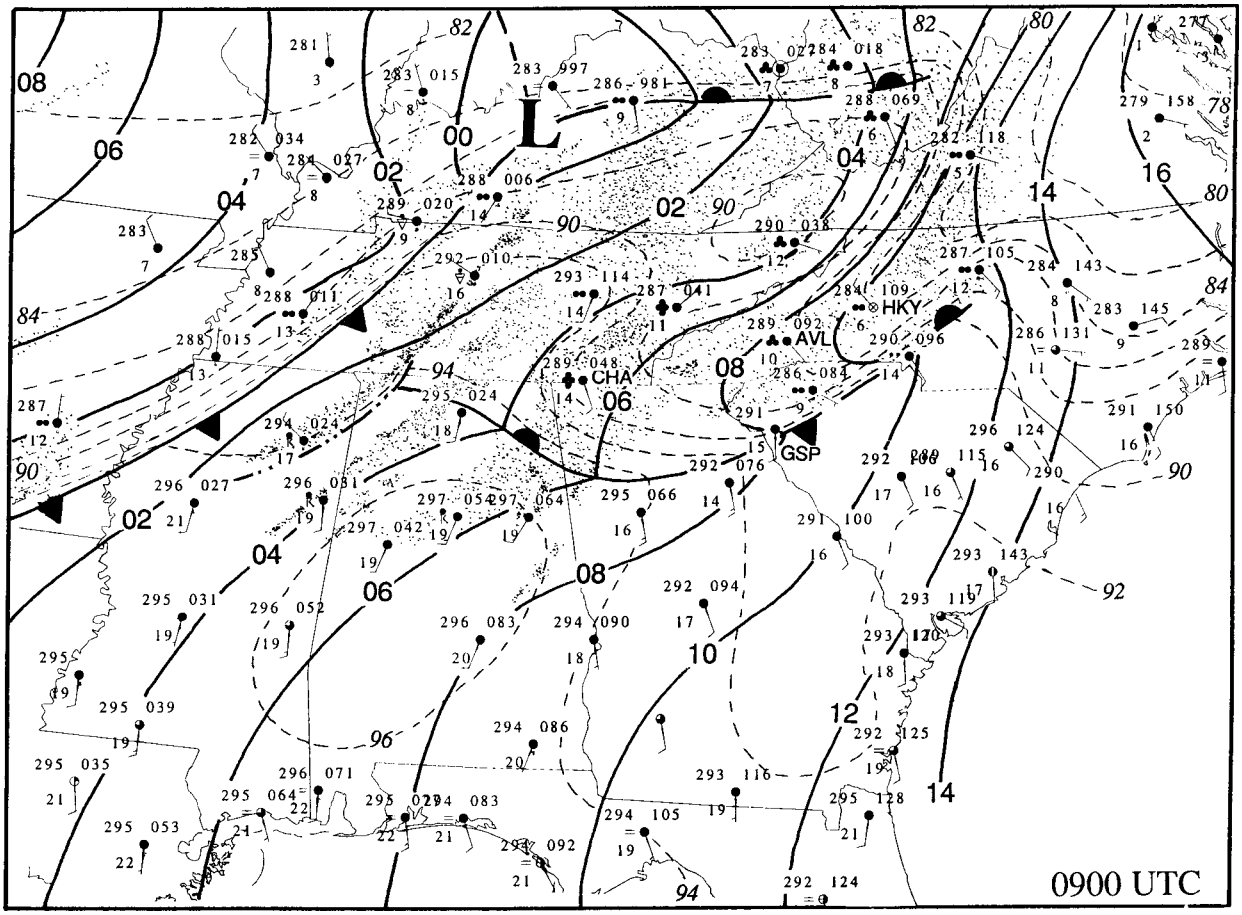

FIG. 5. Same as Fig. 3 but for 0900 UTC and without dewpoint analysis. Stippling indicates areas of precipitation as obtained from a radar mosaic, courtesy of WSI, Inc.

creasing in the warm air to the south. During the 15 h starting at 0000 UTC, a dewpoint ridge pushed east from the Mississippi Valley into Alabama, where, by 1500 UTC, values in excess of 20°C covered half the state. Winds at 925 mb at 1200 UTC were from the south and southwest at roughly 15 m s^{-1} across the region, suggesting the importance of horizontal advection of moisture at low levels during the night.

This case benefits from a supplementary sounding taken at 1800 UTC from Centreville, Alabama (CKL), especially since the site was less than 50 km south of the first convection leading to the long-lived Cherokee County tornadic supercell. Detailed analysis of the lower portions of the temperature soundings for 1200 and 1800 UTC is illustrated in Fig. 10. Surface warming and moistening after 1200 UTC dramatically reduced the static stability of the lowest layers as might be expected, but surprisingly, apparent subsidence was building a cap between 750 and 800 mb.

Evidence for the subsidence can be traced to adiabatic warming and consequent lowering of 1200 UTC stable layers at 700, 750, and 850 mb. Most prominent at 1800 UTC is the inversion layer near 800 mb that appears to have descended about 50 mb in 6 h. There are no observations to tell whether the subsidence was steady over the 6 h, but assuming it was, one can obtain a rough estimate of the temperature profile at 1500 UTC just after convection began. The interpolated profile for 1500 UTC is included in Fig. 10.

Independent evidence of strong vertical motions in this area is provided by the numerical simulation results presented in this issue by Kaplan et al. (1998) and Koch et al. (1998). They show that a low-level jetlet approaching northwest Alabama was associated with maximum descent at about 600 mb. With allowance for some spatial and temporal differences between the simulated and observed fields, the subsidence implied in Fig. 10 may be evidence of displacements due to the approaching jetlet.

Observed mixing ratios averaged over the lowest 50 mb at 1200 and 1800 UTC along with values for 1500 UTC deduced from nearby surface reports are included in Fig. 10. With this information, it is immediately obvious that conditions at 1200 UTC were too stable to

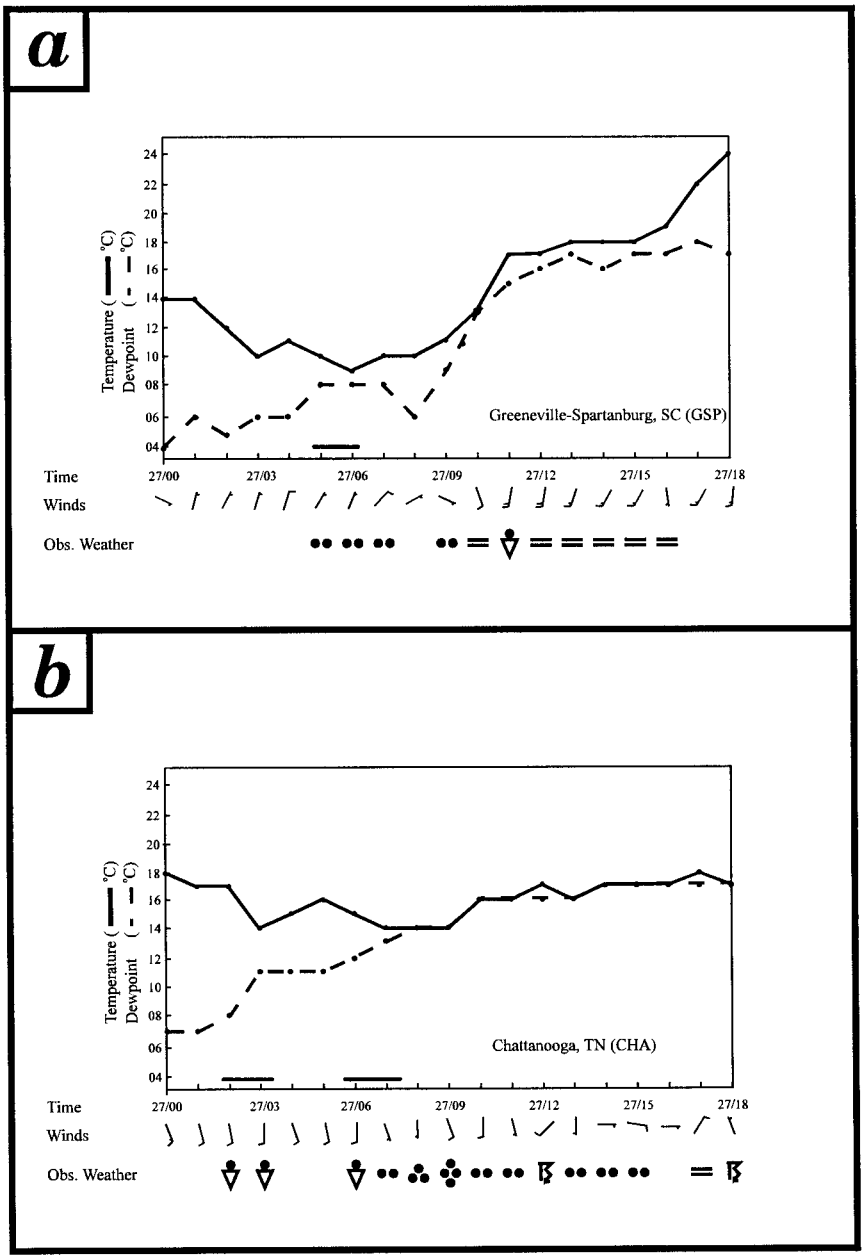

FIG. 6. Time series of temperature (solid, °C) and dewpoint (dashed, °C), winds (kt), and present weather from 0000 to 1800 UTC 27 March at (a) Greenville–Spartanburg, SC (GSP), and (b) Chattanooga, TN (CHA). Bold horizontal lines above each time axis indicate when evaporative cooling may have been occurring.

allow a surface parcel to reach its level of free convection (LFC). Parcels originating from near 940 mb reach the LFC at about 900 mb, and perhaps just penetrate the stable layer at 850 mb. However, throughout its ascent, the saturated parcel remains only slightly warmer than the environment.

By 1500 UTC, temperatures and dewpoints near Birmingham, Alabama (BHM), and CKL increased enough to allow an undiluted surface parcel to just clear the descending cap near 770 mb. By 1800 UTC, the cap was likely stronger, but both surface heating and moistening had compensated to allow a surface parcel to pass through the stable layer. By this time, the convective available potential energy (CAPE) was 2665 J kg^{-2}, with deep convection likely, especially along the dewpoint ridge where the destabilizing contribution of water vapor was a maximum. By 1500 UTC, this ridge extended into central Alabama.

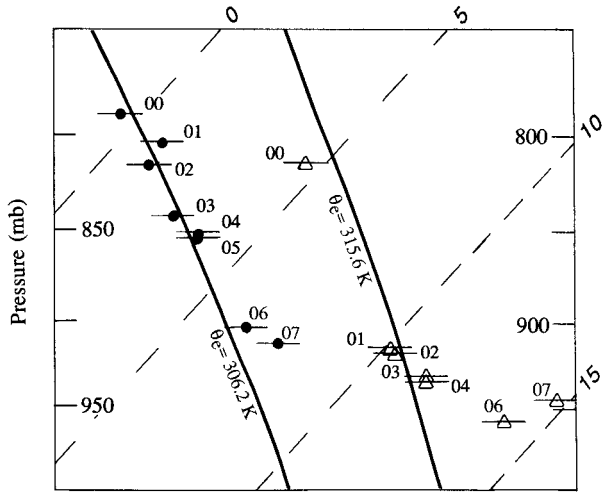

FIG. 7. Time series of saturation points of surface air parcels at Nashville, TN (dots), and Hickory, NC (triangles), plotted on a skew *T*–log*p* diagram. Times are listed in hours UTC. Isotherms are labeled in °C.

c. Storm-scale factors leading to supercell development

By roughly 1500 UTC, the front in Alabama marked the northern boundary of air of decreasing static stability where surface heating and moistening had become sufficient to allow free convection to begin. A radar mosaic at 1445 UTC (Fig. 11) shows widespread precipitation with embedded showers and thunderstorms mostly northwest of the cold front in western Tennessee and northern Mississippi. In addition, two roughly parallel lines of convection in the warm air lay to the southeast. The line at the Mississippi–Alabama border was the more prominent of the two and formed near the extrapolated position of the old outflow boundary seen at 1200 UTC. Hereafter this mesoscale convective system will be referred to as MCS 1A. Just after 1700 UTC, cells in this line began producing tornadoes, including an F2 and an F4 tornado later in northeast Alabama. The second, shorter, and less-developed line of convection seen at 1445 UTC moved on a track nearly parallel to MCS 1A and remained to its south. This second system, hereafter called MCS 2A, included the Cherokee County supercell, which generated at least four violent

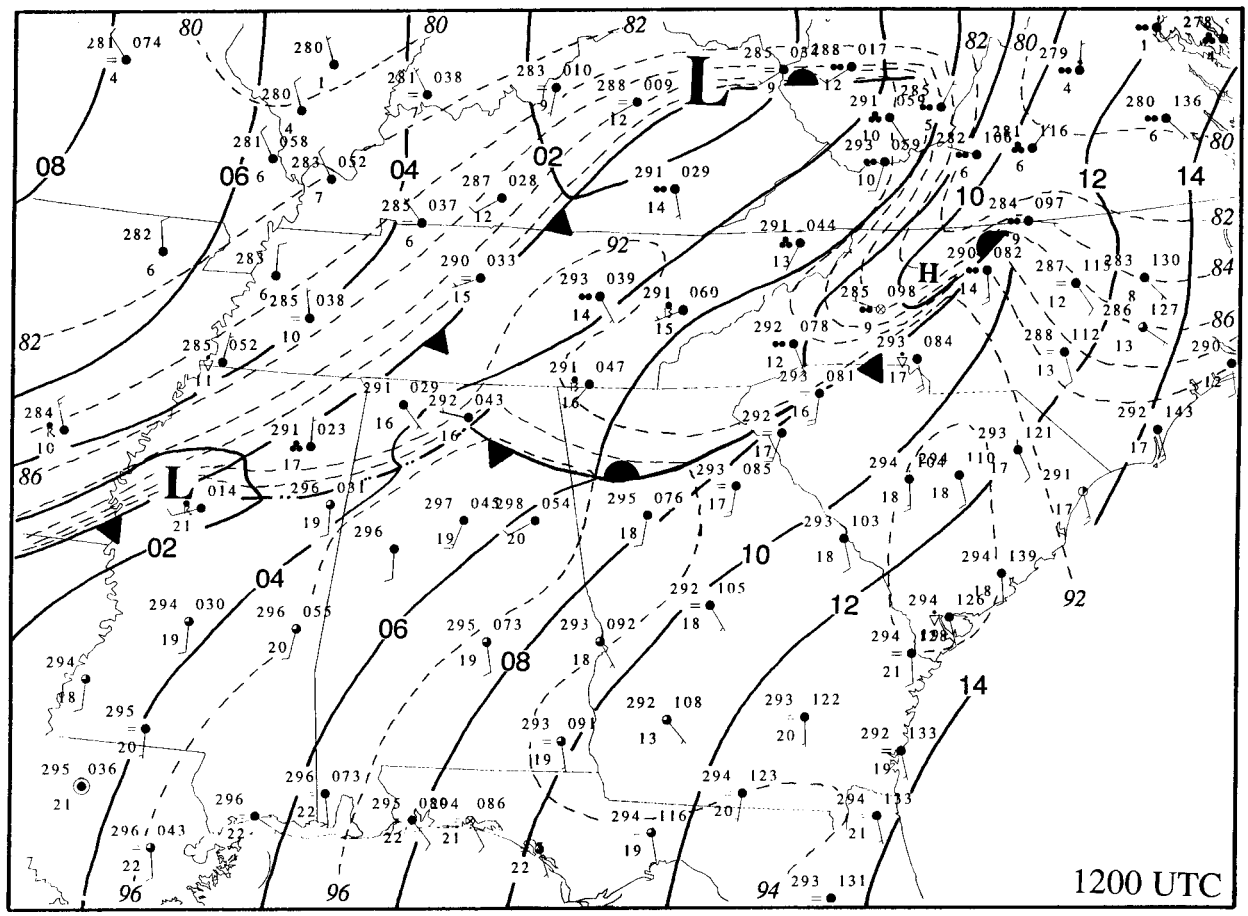

FIG. 8. Same as Fig. 3 but for 1200 UTC and without dewpoint analysis.

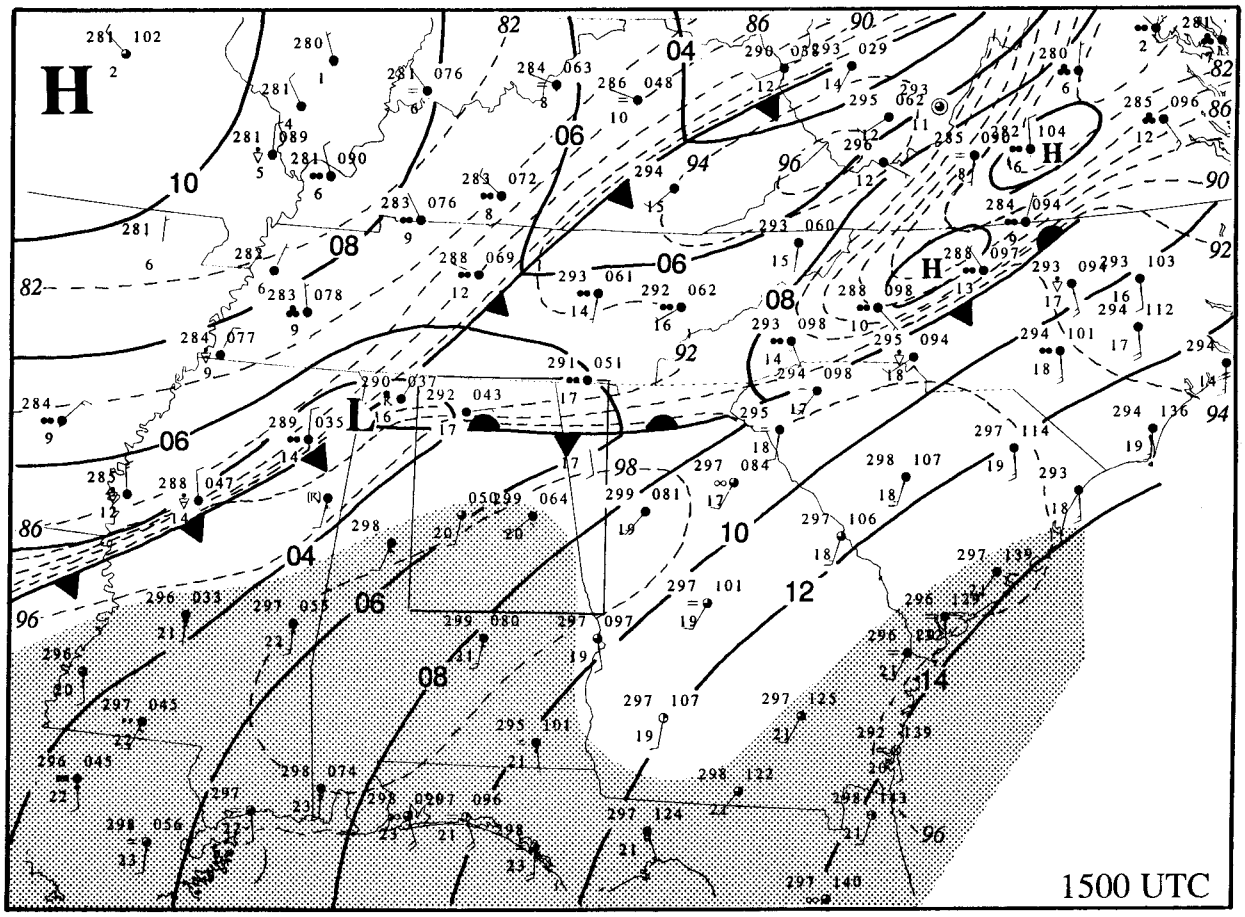

FIG. 9. Same as Fig. 3 but for 1500 UTC. The rectangle in northeast Alabama outlines the area shown in Fig. 12.

long-track tornadoes starting in northeast Alabama and ending more than 3 h later in northwest South Carolina (NOAA 1994a,b).

The purpose of this section is to present observational evidence to help explain why both storm systems intensified to become tornadic supercells and why the Cherokee County storm maintained its intensity for so long.

The first hint that intensification was likely was that both storms were moving toward the front that was positioned just to the north. However, closer examination shows that the cells intensified well south of the frontal convergence and thermal gradient. At 1600 UTC, the northeast member of MCS 1A was in central Alabama and was closest to the front (see Fig. 12). In the next hour, the cell intensified and produced the F2 tornado at 1702 UTC. To its south, the core of the Cherokee County storm in MCS 2A had intensified just a few minutes earlier and produced an F4 tornado at 1655 UTC. The frontal location in northeast Alabama is probably accurate to within 25 km, since it passed RSA, just south of Huntsville, at between 1545 and 1600 UTC when a rapid warming ended and the wind shifted to south. At Huntsville (the northernmost station plotted in Fig. 12) the potential temperature increased 5 K and the wind shifted to south between 1500 and 1600 UTC. Thus, by 1600 UTC, the convergence and strong thermal gradient were along and north of the frontal demarcation of Fig. 12. One should note that the maximum temperatures plotted and analyzed in Fig. 12 are, by definition, nonsynoptic. Thus, the resulting thermal gradient will not coincide with a moving front, as, for example, in extreme northeast Alabama and northwest Georgia where the front evidently continued moving north after 1600 UTC.

It might be argued that, based on the thermal gradient, the front should be analyzed about 100 km farther south. However, the magnitude of the gradient there is only about half that found farther north. Furthermore, extensive cloudiness associated with supercell development and evaporation from the wet surface likely reduced solar heating after midmorning, thus creating the southern gradient.

Diurnal surface warming and moistening that had already taken place up until 1500 UTC were almost certainly major contributors to storm intensification. Recall that several rainbands had crossed northern Alabama during the preceding 10 h. Rain gauges recorded over

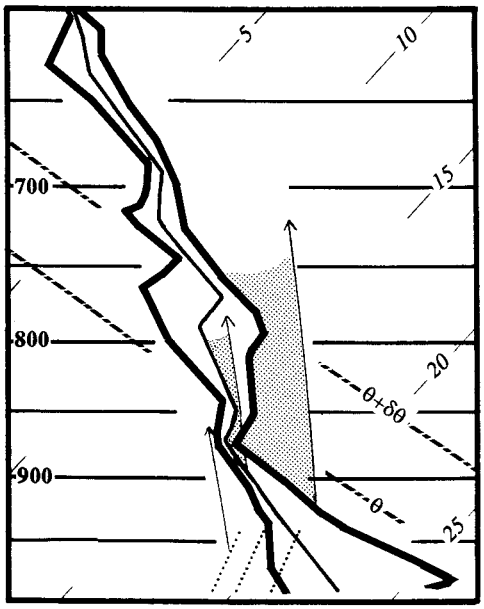

FIG. 10. Skew *T*–log*p* chart of the temperature profiles at Centreville, AL (CKL), at 1200 and 1800 UTC as illustrated by left and right heavy solid lines, respectively. The 1500 UTC profile (center line) is interpolated. Mixing ratios averaged through the lowest 50 mb at 1200, 1500, and 1800 UTC are depicted by dotted lines from left to right at the bottom of the diagram. Paths taken by undiluted surface parcels for each time are illustrated by arrows with initial zones of positive buoyancy included as stippled areas.

2 cm of precipitation across most of that region. The broad dashed line in Fig. 12 defines the approximate southern limit of the wet surface. As warm air streamed north across the line, it began advancing over progressively wetter ground. Thus, both storms at 1600 UTC were either in or about to move into areas where surface moisture available for evaporation was abundant. However, due to the lack of surface hourly reports from this area, the amount of water vapor enhancement of storm inflow remains speculative.

Finally, by about 1500 UTC, large breaks began developing in the overcast cloudiness that had been widespread across the state. These breaks can be seen in the morning *GOES-7* imagery presented in this issue by Koch et al. (1998). Ensemble-averaged solar radiation values at the RSA network increased from near zero at 1415 UTC to 441 W m^{-2} at 1545 UTC, showing that solar input increased even under mostly cloudy skies. At the latitude of northern Alabama on 27 March at 1545 UTC, the total solar radiation incident on a horizontal surface at the top of the atmosphere, and thus the total possible radiation, is 979 W m^{-2}. With mostly sunny skies, as would be characteristic of the open areas across sections of eastern Alabama, the solar input at the surface would likely have been in the neighborhood of 600–700 W m^{-2}. With such an energy input, appreciable surface heating was likely in some areas for 1–2 h prior to the first round of deep convection and its associated dense cloud cover. The northward extension of the area of maximum temperature of over 26°C in eastern Alabama in Fig. 12 provides at least some evidence of solar heating.

Storm-relative helicity based on the observed storm motion vector of 245° at 23 m s^{-1} and the observed winds from the CKL sounding at 1800 UTC was 443 m^2 s^{-2}. Although not exceptional, along with the large CAPE value, this helicity was strong and supportive of supercell formation. [See Johns and Doswell (1992) for values associated with strong and violent tornadoes.] Strong south-southwesterly flow of up to 20 m s^{-1} in the PBL fed the storms from their southeast flanks (Fig. 12, inset).

Both major cells in MCS 1A and 2A intensified as they moved east-northeast. The cores of both storm cells became best defined with strongest radar reflectivities when they were just north of their F4 tornado tracks starting at 1655 and 1732 UTC, respectively. However, much of the leading end of MCS 1A quickly dissipated at about 1800 UTC.

Two factors may have contributed to the rapid demise of the northern cell: 1) it may have had its inflow cut off by MCS 2A and 2) it crossed the warm front. To consider the first possibility, let us assume that the wind of 195° at 16 m s^{-1} as measured at $z = 361$ m at CKL was representative of conditions over northeast Alabama. An air parcel moving at this velocity and entering the dying northern cell at 1800 UTC would have originated near the northern edge of MCS 2A an hour earlier as it was producing its first tornado (see Fig. 13). Thus, it is quite possible that 2A redirected much of the warm moist flow into its updraft and led to starvation of cell 1A. One can also see in Fig. 13 that at 1700 UTC, when the northern cell was part of a well-developed line, it was sufficiently removed from rapidly developing MCS 2A that its low-level inflow for roughly the next hour would have originated north of MCS 2A.

Between 1745 and 1815 UTC, the core of the northern storm can be seen quickly dissipating north of the front (Fig. 14). Vertical circulations normally associated with frontal zones should enhance convection at least immediately at the front. The observations do not rule out rapid brief intensification, since a strong well-organized core is evident within 5–10 km of the front and hence within the uncertainty of its location. As the storm continued northeast and moved farther into the cold air, its moist inflow layer likely became increasingly elevated above the frontal surface. Furthermore, stable air below may have become involved in the updraft.

Meanwhile, the Cherokee County supercell in MCS 2A, to the southeast, had pulsed to its second reflectivity maximum and was about to produce its second tornado. The subsequent path of this supercell brought it roughly along and parallel to the frontal boundary as best deduced from surface observations. As in the case of the northern storm complex, radar reflectivities of portions of the southern system that crossed the warm front dissipated rapidly.

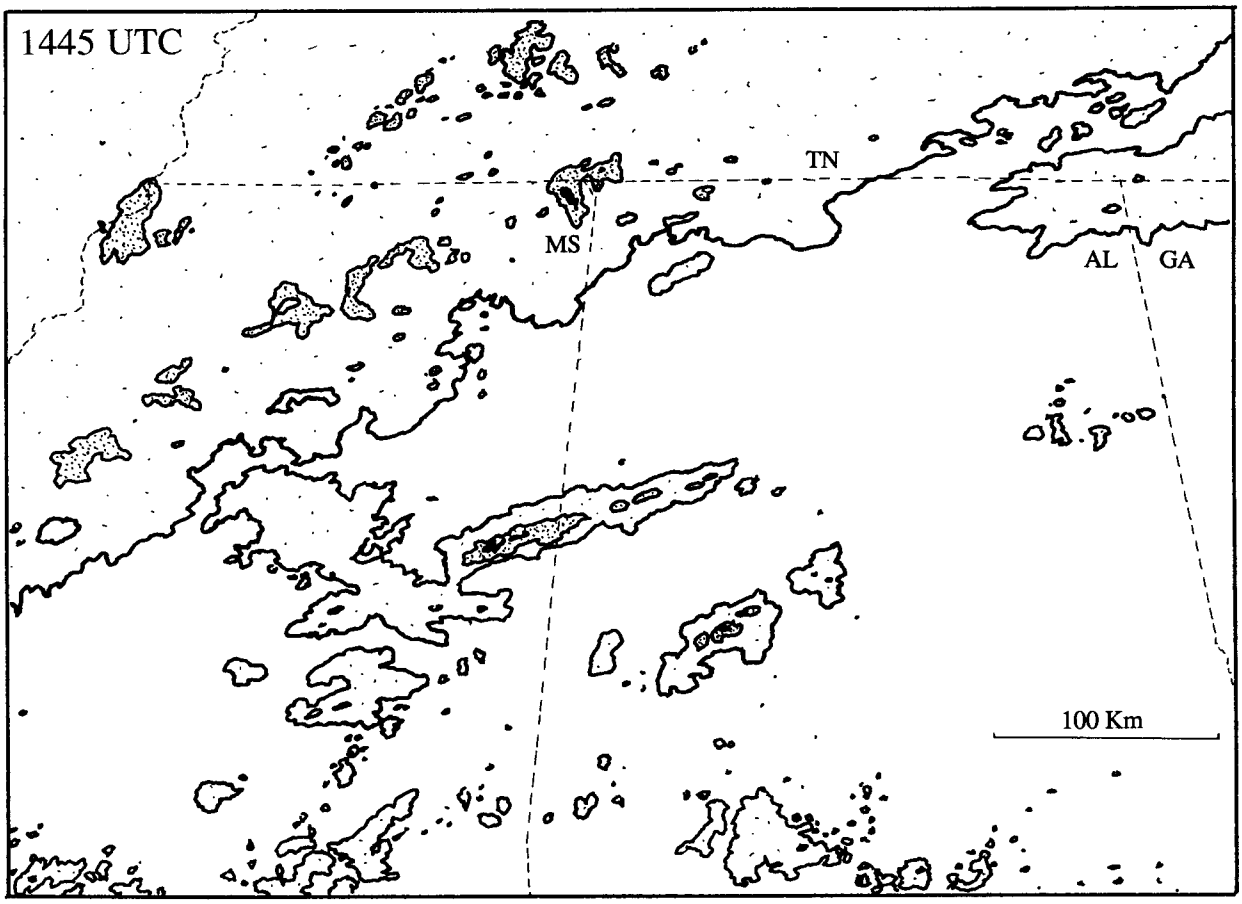

FIG. 11. Radar mosaic at 1445 UTC. Reflectivities of 10–30 dB*Z* and 41–45 dB*Z* are illustrated by light and moderate stippling, respectively. Reflectivities of 51 dB*Z* or more are shown by solid areas. Information obtained from WSI mosaic and radar imagery supplied courtesy of K. Knupp, University of Alabama at Huntsville.

Mesoscale surface analyses at 1800 and 2000 UTC (Fig. 15) show the location of the front and the core of the Cherokee County supercell (MCS 2A) moving along the frontal boundary in northern Georgia. The front had maintained its strength despite the gradual breakdown of the in situ damming over western North Carolina. Partial clearing evident from satellite imagery and station reports south of the front at 1800 and 2000 UTC contrast with solid overcast and reports of precipitation to the north. This contrast and associated temperature differences suggest that differential diurnal heating across the front was the major contributor to maintenance of the thermal gradient. The temperature and pressure fields near the strong convection are only approximate in Fig. 15 due to the limited surface observations. For example, isotherms were analyzed assuming that cyclonic rotation near supercells was reflected in the thermal field, but the amplitude of temperature and pressure fields near these systems may have been underrepresented. Nevertheless, one can see that a mesoscale surface low was approaching from the west along the front and that the convection was associated with the low. Southeast of the low, the pressure gradient was stronger than farther east and was associated with backed (i.e., more southerly) winds. If we assume a continued southwesterly flow aloft, as in Fig. 12 (inset), the backed winds locally enhanced the storm-relative inflow and maintained high helicity just ahead of MCS 1 and 2.

The relationship between the front and the supercells changed at about 1800 UTC. Prior to that time, the storms were approaching the front at a 30°–40° angle. But afterward, as, for example, when the MCS 2A moved into Georgia, their motion coincided with the frontal alignment to within 10°–20°. This change was largely due to the gradual curvature of the front around the southern flank of the Appalachians as was common to all surface analyses presented here. By 1800 UTC the frontal orientation of roughly 250°–260° (Fig. 14a) approximated that of the storm motion. One would expect upward vertical motion along the front to contribute to convection and help maintain a supercell once it became coupled with the front. Evidently the coupling contributed to the sustained severity of the Chrokee County supercell, since it continued producing severe, long-track tornadoes including the F4 Indian Springs

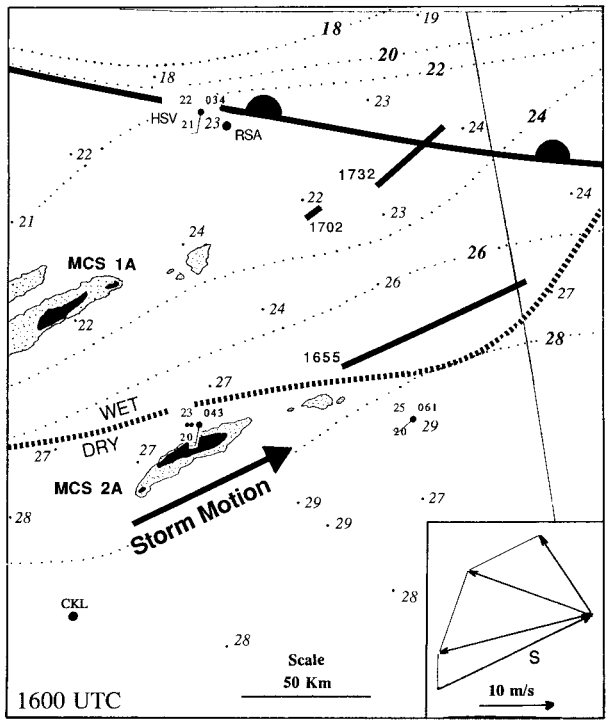

FIG. 12. Composite diagram for 1600 UTC over northeast Alabama and extreme northwest Georgia (see Fig. 9) including location of surface warm front, the cores of MCS 1A and 2A (with 41–45 dBZ, stippled, and 51 dBZ or more, solid). The broad dashed line represents the isopleth of 0.5 cm of rainfall accumulated since 0500 UTC. Tornado tracks are illustrated by solid straight lines with the time of first-reported tornado touchdown given in UTC. Isotherms of 24-h maximum temperature are illustrated by dotted lines labeled in °C. Full station plots are in the same format as Fig. 3 except that temperatures are plotted in °C. Plots of maximum temperatures from the cooperative network are expressed in °C (italics). Radar information was supplied courtesy of K. Knupp, University of Alabama at Huntsville. The inset at the lower right depicts the hodograph of observed storm motion (S) and the storm-relative flow at $z = 10$, 361, and 861 m above the surface as computed from the 1800 UTC sounding at CKL.

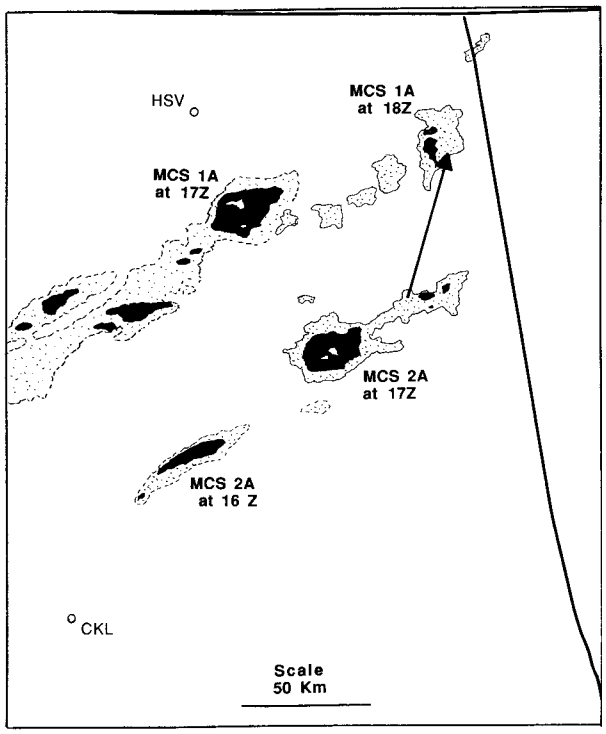

FIG. 13. Time series of radar reflectivity cores for MCS 1A and 2A at selected hourly intervals. The arrow depicts a 1-h displacement for air parcels at a height of 361 m ending at MCS 1A at 1800 UTC. The area shown is the same as Fig. 12.

tornado and the F3 Dahlonega tornado each of which had pathlengths through northern Georgia of over 70 km. In Fig. 15, MCS 1 west-southwest of the Cherokee County supercell (MCS 2A) is seen also moving parallel to the front. This cell produced the 64-km-long Henderson Mountain tornado starting at 2001 UTC and the 37-km-long Cleveland tornado at 2023 UTC, both of F3 intensity. In fact, both supercells produced additional subsequent tornadoes and numerous reports of hail of 4–5-cm diameter in northeast Georgia and northern South Carolina, right along the frontal boundary. Finally, a third supercell crossed the Alabama–Georgia line just minutes prior to 0000 UTC on 28 March, following the same track as the previous two supercells. It produced an F1 and a long-track F3 tornado. This last supercell was associated with a separate broken northeast–southwest-oriented line of cells just ahead of the cold front. Further information documenting the radar structure of individual cells of the outbreak has been presented by Knupp et al. (1996).

5. Summary and conclusions

Supercell thunderstorms associated with the deadly Palm Sunday 1994 tornado outbreak developed and evolved in response to a variety of diabatic mesoscale processes including differential evaporative cooling and solar heating. The resulting instability in an environment with strong storm-relative helicity resulted in supercell formation by midmorning of 27 March over central and northern Alabama.

The northern limit of the unstable conditions was defined by a shallow east–west frontal boundary, which formed and was maintained chiefly by diabatic processes. During the previous night, widespread moderate to heavy precipitation fell into dry air over the Tennessee Valley and spread across the mountains into western North Carolina where surface wind and pressure fields showed that limited cold air damming was occurring. Evaporation cooled the air across much of the region north of the weak front. In the foothills and piedmont east of the mountains, a cool high pressure ridge strengthened and helped define the front across the Carolinas and apparently led to a cool drainage flow strengthening the front across northern Georgia. Farther west in northern Alabama, the front was less well de-

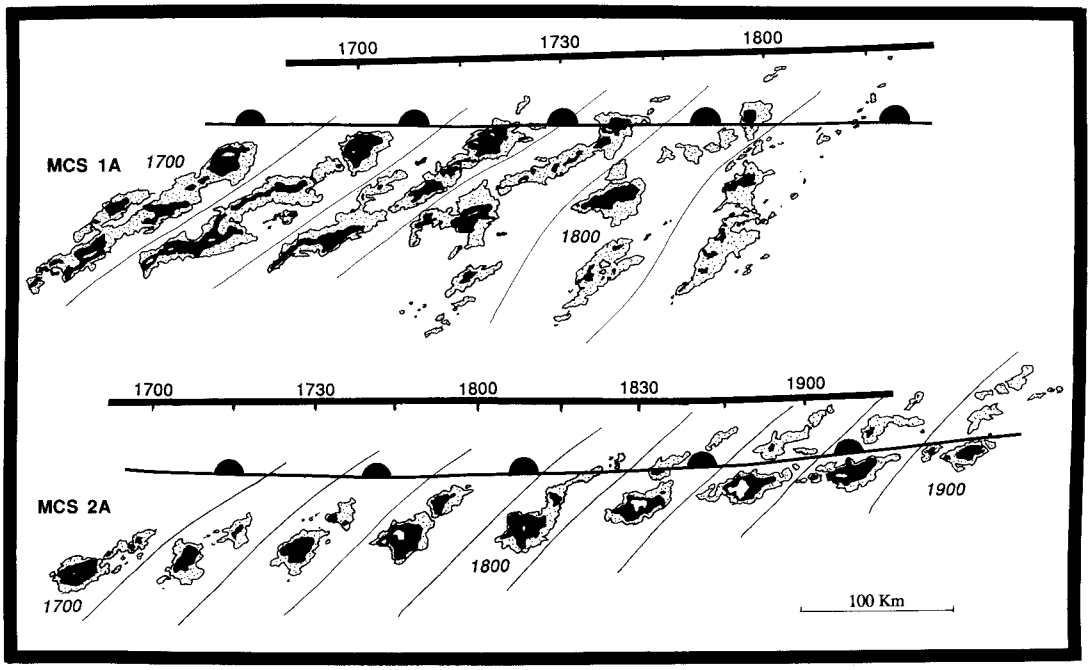

FIG. 14. Time series of composite reflectivity showing motion of reflectivity cores relative to the warm front. Reflectivities of 41–45 dB*Z* (stippled), 51–57 dB*Z* (solid), and greater than 57 dB*Z* (white) are shown for MCS 1A (top) and 2A (bottom). The latter includes the Cherokee County supercell. Core locations are given at 15-min intervals with depictions at each hour labeled in UTC. The bold solid line above each series represents the southern border of Tennessee with pips labeled every half hour (UTC) to represent the point where the Alabama–Georgia–Tennessee borders intersect. Radar imagery used in this analysis was supplied by K. Knupp.

fined until after cool outflow from a convective line helped promote frontogenesis. After sunrise, temperatures to the south of the front increased through solar heating, while to the north, cooler temperatures were sustained by solid cloud cover and precipitation. The resulting differential heating along with thermal advection south of the front strengthened the boundary, which remained practically stationary throughout the day.

Analysis of sounding data showed that strong subsidence centered at about 800 mb during the morning hours may have capped convection prior to about 1500 UTC, but strong surface heating and moistening across central Alabama compensated at about that time. Further heating and moistening then led to high values of CAPE contributing to strong updraft development.

Only circumstantial evidence could be found to explain the location of initiation of the daytime convection that was to evolve into the tornadic supercells. A primary line of thunderstorms formed in northwest Alabama possibly along the preexisting outflow boundary that had moved close to that area. A second, shorter complex that later led to the Cherokee County supercell formed to the southeast of the primary line. Both lines may have formed in response to dynamics associated with the low-level jetlet, which numerical simulations show was approaching that location at roughly that time (see Koch et al. 1998). The low-level subsidence deduced from the soundings was evidence of such a low-level dynamic feature.

Once the two initial convective systems formed, they moved toward an area that had been well moistened by rainfall. The moist surface may have provided a source of evaporation, as large breaks in the overcast allowed appreciable solar heating in the area of storm inflow. Both storms became tornadic as they moved across the wet surface and approached within 25 km downwind of the cloud breaks.

After producing two tornadoes, the northern cell of the initial line (MCS 1A) disintegrated as its flow likely became blocked by its southern neighbor (2A) and as it crossed the front. However, the Cherokee County storm (2A) and the supercell that later formed behind it continued to generate tornadoes throughout much of the afternoon as they moved through northern Georgia and South Carolina. Here the frontal orientation had changed to match the storm motion to within 10°–20°. Both storms intersected the front and moved along it for several hours. Well-developed southerly flow, apparently maintained by the approaching mesolow, and enriched by continued solar heating, provided a continued inflow of unstable air with high helicity for both cells.

This case resembles Miller's (1972) ''warm advection pattern'' described briefly by Johns and Doswell (1992).

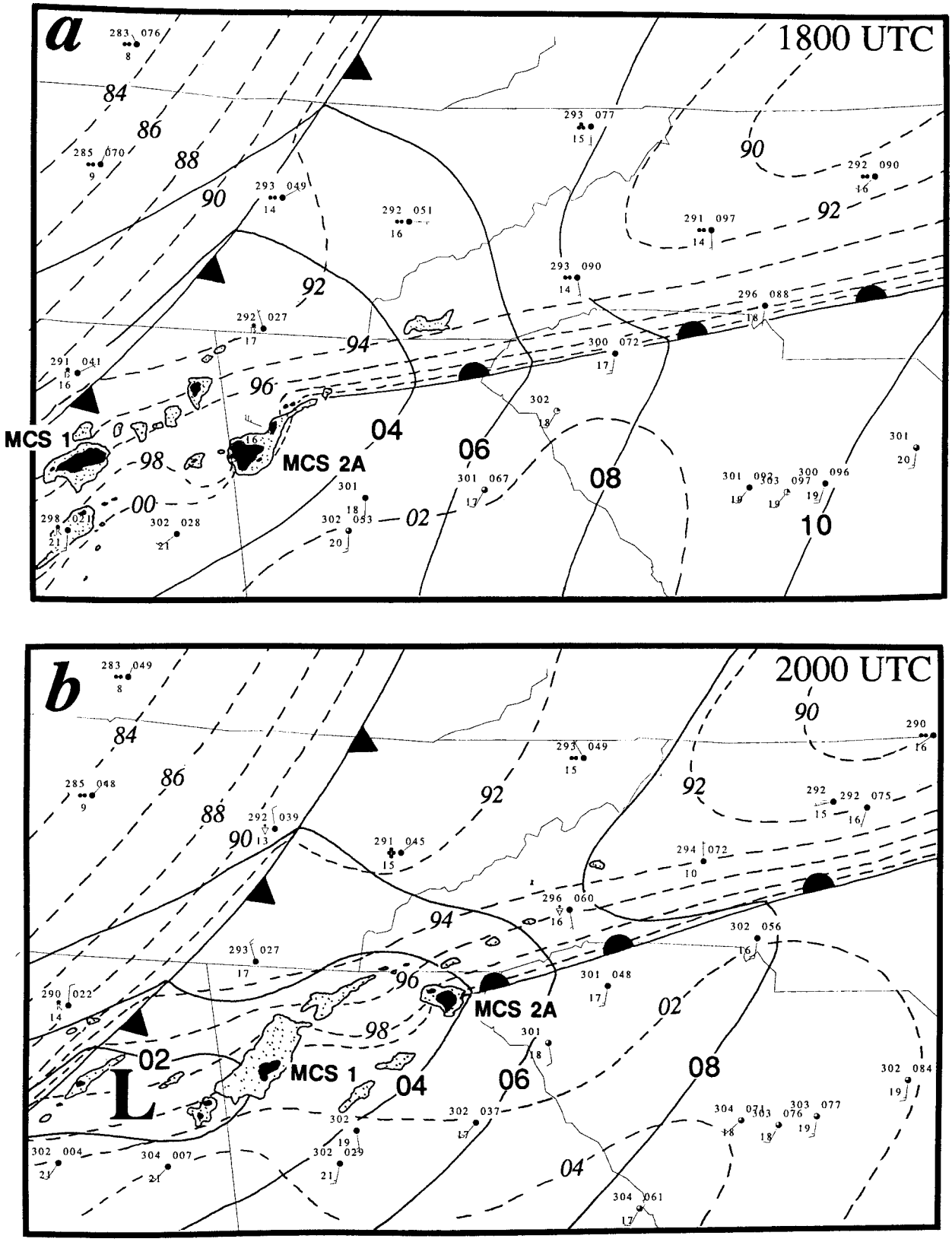

FIG. 15. Surface analysis of sea level pressure (solid lines labeled in mb) and potential temperature (dashed lines labeled in K) for (a) 1800 UTC and (b) 2000 UTC. Also included are reflectivity cores of MCS 1A and 2A. Reflectivities of DVIP 3 are stippled and 5 are solid. Radar imagery used in this analysis was supplied by K. Knupp.

In this synoptic pattern, tornadic storms occur near a roughly stationary or warm front oriented parallel to the midlevel wind. Sometimes in this pattern severe weather is associated with only a weak short wave. In our case, classic midlevel forcing was not evident (Koch et al. 1998) and the midlevel flow was roughly parallel to the front. What makes this outbreak unusual is that the front was a shallow feature mostly formed and maintained by processes that are normally considered ancillary or secondary to synoptic-scale processes. The role of evaporative cooling, damming, and differential heating due to cloud cover seemed to be dominant in our case.

The conceptual model presented by Maddox et al. (1980) appears to be relevant in explaining initial supercell development in our case. They suggested that destabilization by significant evaporation from a wet surface left by an advancing warm front can be important in enhancing convective instability in the warm air, particularly if solar radiation contributes to warming. They hypothesized that such surface modification may explain why storms often become tornadic as they approach warm frontal boundaries.

The maintenance of intense thunderstorms as they move along warm or stationary fronts has long been noted by investigators (e.g., Magor 1959; Miller 1972). Maddox et al. (1980) presented surface mesoscale analyses of eight tornado cases and showed that thunderstorms that move along thermal boundaries produce intense long-track tornadoes, while those that cross the boundaries produce intense but short-track tornadoes. Such storm behavior is exactly what was observed in our case where one convective complex crossed the frontal boundary, stopped producing tornadoes, and quickly dissipated. However, it was not clear that this convection intensified at the front as is conventional wisdom and as Maddox et al. (1980) and Imy et al. (1992) found. Some cell strengthening immediately at the front could not be ruled out in our case, however, because of uncertainty in the exact frontal location.

In the case presented here, the Cherokee County supercell and those that followed along similar tracks all developed sufficiently south and east to intersect and move along the frontal boundary. These storms then produced a succession of severe and devastating tornadoes over a narrow swath of over 200 km in length. Thus, by implication, the alignment of storm motion with the thermal boundary was a key factor in storm maintenance and helps explain the narrow width of the outbreak.

This study suggests that many observed aspects of supercell evolution can be reasonably explained by comparing storm motion with frontal orientation, the location and intensity of upstream cells, and the locations of downstream areas where enhanced surface heating and/or moistening are likely. To be useful in forecasting, such comparisons would require the ability to combine detailed mesoscale surface analysis with current radar and satellite imagery.

There are still many unanswered questions that need to be investigated to link storm dynamics to the mesoscale environment. For example, at what approach angle do storms dissipate rather than intensify as they encounter a frontal boundary? One could immediately argue that the answer depends not only on the approach angle, but on the storm dynamics, the nature of the boundary, and the wind, temperature, and moisture structure of the storm's environment. For example, storm motion is partly controlled by advection and partly by new echo development. If stability and storm-relative inflow are favorable for rapid development, the storm approach angle may not be as critical in producing storm motion along the front. Another question suggested by this study involves the role of evaporation and surface heating in destabilizing the lower atmosphere and triggering or enhancing convection. Such surface processes need to be quantified and reliably simulated to provide understanding and useful real-time forecast information.

A denser network of surface sites with frequent measurements of standard variables would be most helpful in beginning to address such questions. Station spacing of roughly 50 km and reporting intervals of 5 min, as is used by the Oklahoma mesonet, for example, would provide much needed detail. Availability of solar and net radiation measurements and instrumentation to monitor or estimate surface energy fluxes would also be very helpful. This study benefited greatly from the supplemental 1800 UTC sounding since it allowed assessment of changing stability and helicity. Wind profiler data and Doppler-derived velocity fields and VAD wind profiles from the WSR-88D network will continue to be most helpful in studies of future outbreaks.

Acknowledgments. The authors are grateful to a number of contributors from the Southeast Consortium on Severe Thunderstorms and Tornadoes. Radar and mesonet data were kindly provided by Kevin Knupp. Doug Schneider of the North Carolina State Climate Office furnished data from the cooperative observer network. Thanks also are extended to Chuck Doswell and other reviewers for their helpful comments and suggestions. This research was supported by the National Oceanic and Atmospheric Administration through Grant NA 57RAO482.

REFERENCES

Barnes, S. L., 1973: Mesoscale objective analysis using weighted time-series observations. NOAA Tech. Memo. ERL NSSL-62, Norman, OK, 60 pp. [NTIS COM-73-10781.]

Bell, G. D., and L. F. Bosart, 1988: Appalachian cold-air damming. *Mon. Wea. Rev.*, **116,** 137–161.

Betts, A. K., 1982: Saturation point analysis of moist convective overturning. *J. Atmos. Sci.*, **39,** 1484–1505.

——, 1984: Boundary layer thermodynamics of a high plains severe storm. *Mon. Wea. Rev.*, **112,** 2199–2211.

Businger, S., W. H. Bauman, and G. F. Watson, 1991: The devel-

opment of the Piedmont front and associated severe weather on 13 March 1986. *Mon. Wea. Rev.,* **119,** 2224–2251.
Dorian, P. B., and S. E. Koch, 1988: Mesoscale frontogenesis as a predictor of squall line initiation. Preprints, *15th Conf. on Severe Local Storms*, Norman, OK, Amer. Meteor. Soc., 364–367.
Fritsch, J. M., J. Kapolka, and P. A. Hirschberg, 1992: The effects of subcloud-layer diabatic processes on cold air damming. *J. Atmos. Sci.,* **49,** 49–70.
Gyakum, J. R., and E. S. Barker, 1988: A case study of explosive subsynoptic-scale cyclogenesis. *Mon. Wea. Rev.,* **116,** 2225–2253.
Hamilton, D. W., Y.-L. Lin, R. P. Weglarz, and M. L. Kaplan, 1998: Jetlet formation from diabatic forcing with applications to the 1994 Palm Sunday tornado outbreak. *Mon. Wea. Rev.,* **126,** 2061–2089.
Imy, D. A., K. J. Pence, and C. A. Doswell III, 1992: On the need for volumetric radar data when issuing severe thunderstorm and tornado warnings. *Natl. Wea. Dig.,* **17,** 2–17.
Johns, R. H., and C. A. Doswell III, 1992: Severe local storms forecasting. *Wea. Forecasting,* **7,** 588–612.
Kaplan, M. L., Y.-L. Lin, D. W. Hamilton, and R. A. Rozumalski, 1998: The numerical simulation of an unbalanced jetlet and its role in the Palm Sunday tornado outbreak in Alabama and Georgia. *Mon. Wea. Rev.,* **126,** 2133–2165.
Keeter, K. K., S. Businger, L. G. Lee, and J. S. Waldstreicher, 1995: Winter weather forecasting throughout the eastern United States. Part III: The effects of topography and the variability of the winter weather in the Carolinas and Virginia. *Wea. Forecasting,* **10,** 42–60.
Knupp, K., R. Clymer, E. McCaul, and K. Pence, 1996: Structure and evolution of the 1994 Palm Sunday tornadic storms and their near mesoscale environment. Preprints, *18th Conf. on Severe Local Storms*, San Francisco, CA, Amer. Meteor. Soc., 42–46.
Koch, S. E., 1984: The role of an apparent mesoscale frontogenetic circulation in squall-line initiation. *Mon. Wea. Rev.,* **112,** 2090–2111.
——, J. T. McQueen, and V. M. Karayampudi, 1995: A numerical study of the effects of differential cloud cover on cold frontal structure and dynamics. *J. Atmos. Sci.,* **52,** 937–964.
——, A. Aksakal, and J. T. McQueen, 1997: The influence of mesoscale humidity and evapotranspiration fields on a model forecast of a cold frontal squall line. *Mon. Wea. Rev.,* **125,** 384–409.
——, D. Hamilton, D. Kramer, and A. Langmaid, 1998: Mesoscale dynamics in the Palm Sunday tornado outbreak. *Mon. Wea. Rev.,* **126,** 2031–2060.
Korotky, J. D., 1990: The Raleigh tornado of November 28, 1988: The evolution of a tornadic environment. Preprints, *16th Conf. on Severe Local Storms,* Kanasaskis Park, AB, Canada, Amer. Meteor. Soc., 532–537.
Maddox, R. A., L. R., Hoxit, and C. F. Chappell, 1980: A study of tornadic thunderstorm interactions with thermal boundaries. *Mon. Wea. Rev.,* **108,** 322–336.
Magor, B. W., 1959: Mesoanalysis: Some operational analysis techniques utilized in tornado forecasting. *Bull. Amer. Meteor. Soc.,* **40,** 499–511.
Miller, R. C., 1972: Notes on analysis and severe storm forecasting procedures of the Air Force Global Weather Central. Tech. Rep. 200 (revised), AWS, USAF, 181 pp. [Available from Headquarters AWS, Scott AFB, IL 62225.]
NOAA, 1994a: Natural disaster survey report: Southeastern United States Palm Sunday tornado outbreak of March 27, 1994. NOAA Rep., Silver Spring, MD, 54 pp. [Available from NOAA Headquarters, 1335 East–West Highway, Silver Spring, MD 20910.]
——, 1994b: *Storm Data.* Vol. 36, 281–289. [Available from NCDC, Federal Bldg., Asheville, NC 28801-2696.]
O'Handley, C., and L. F. Bosart, 1996: The impact of the Appalachian mountains on cyclonic weather systems. Part I: A climatology. *Mon. Wea. Rev.,* **124,** 1353–1373.
Sanders, F., and C. A. Doswell, 1995: A case for detailed surface analysis. *Bull. Amer. Meteor. Soc.,* **76,** 505–521.
Segal, M., and R. W. Arritt, 1992: Nonclassical mesoscale circulations caused by surface sensible heat-flux gradients. *Bull. Amer. Meteor. Soc.,* **73,** 1593–1604.
——, F. W. Purdom, J. L. Song, R. A. Pielke, and Y. Mahrer, 1986: Evaluation of cloud shading effects on the generation and modification of mesoscale circulations. *Mon. Wea. Rev.,* **114,** 1201–1212.
——, J. R. Garratt, G. Kallos, and R. A. Pielke, 1989: The impact of wet soil and canopy temperatures on daytime boundary layer growth. *J. Atmos. Sci.,* **46,** 3673–3684.
——, W. L. Physick, J. E. Heim, and R. W. Arritt, 1993: The enhancement of cold-front temperature contrast by differential cloud cover. *Mon. Wea. Rev.,* **121,** 867–873.
Sun, W.-Y., and Y. Ogura, 1979: Boundary-layer forcing as a possible trigger to a squall-line formation. *J. Atmos. Sci.,* **36,** 235–254.
Thompson, W. T., and S. D. Burk, 1991: An investigation of an Arctic front with a vertically nested mesoscale model. *Mon. Wea. Rev.,* **119,** 233–261.
Vescio, M. D., K. K. Keeter, G. Dial, P. Badget, and A. J. Riordan, 1993: A low-top reflectivity severe weather episode along a thermal/moisture boundary in eastern North Carolina. Preprints, *17th Conf. on Severe Local Storms,* St. Louis, MO, Amer. Meteor. Soc., 628–632.
Zhang, D.-L., and R. A. Anthes, 1982: A high-resolution model of the planetary boundary layer sensitivity tests and comparisons with SESAME-79 data. *J. Appl. Meteor.,* **21,** 1594–1609.